2024 IEEE/ASME International Conference on Advanced Intelligent Mechatronics (AIM)
July 15-19, 2024. Boston, MA, USA

Development and Control of a Cable-Driven Robotic Platform for Studying Human Balance and Gait

Oluwasegun Akinniyi[1], *Student Member, IEEE*, Mojtaba Sharifi[2], *Member, IEEE*, Dario Martelli[3], Qiang Zhang[1*], *Member, IEEE*

***Abstract*— Aging is one of the main causes of weakness in mobility and a high risk of falling due to the degradation of neuromuscular and skeletal systems. Tremendous cable-driven robotic assistive devices have been proposed in recent years with the goal of fall risk mitigation and rehabilitation interventions. However, most of them require sophisticated structure and mechatronics design, leading to a relatively bulky nature. In this study, we developed a cable-driven robotic platform for waist perturbation. A lightweight load cell is installed between the end of the cable and a wearable waist belt to measure the pulling force in real time. A closed-loop adaptive full-state feedback control with reference input is proposed to guarantee good torque trajectory tracking performance. Preliminary benchtop and human subject testing with the proposed controller demonstrated an improved force tracking performance of sinusoidal force profiles ranging from 20 N to 80 N, with Root Mean Square Error (RMSE) values of 2.6 N to 10.6 N during fixed-object perturbations and 3.4 N $\pm$ 0.2 N to 12.7 N $\pm$ 1.0 N during standing perturbations, respectively, as compared to a RMSE of 5.6 N to 21.4 N and 7.1 N $\pm$ 0.6 N to 33.7 N $\pm$ 2.9 N with the traditional proportional-integral-derivative controller using the same force profile and magnitudes, and under the same perturbation conditions. The hardware and control development of this robotic platform will be used for balance perturbation studies during static standing and human-in-the-loop optimization control studies during dynamic walking tasks.**

I. Introduction

Falls are a leading contributor to injury and hospitalization among older adults [1]. One in three adults above 65 falls once a year, leading to injury, traumatic and psychological consequences, or death [2]. Fall-related accidents in the U.S. cost the healthcare system about $50 billion dollars a year [3]. Therefore, improved fall-prevention technologies are quite important for society.

Most falls are due to internally generated errors and external bumps leading to undesirable center of mass (COM) movement [4]. The most common fall conditions in older adults living in care facilities include slips, trips, bumps, and incorrect weight shifting [5]. One of the causes of loss of balance and reduced gait function in older adults is the decline in muscle strength in the lower limb [6]. The application of external perturbations on the COM could be used in balance recovery training where subjects can improve their balance in response to repeated waist perturbations, consequently reducing the number of falls in real life.

Recent trends in COM-related falls and the advantages of studying falls in the laboratory have led to an increase in the development and use of robotic devices for fall risk reduction interventions and rehabilitation [7]. Researchers use these devices to simulate real-world fall conditions like hits, bumps, and incorrect weight shifting in the laboratory, safely applying physical perturbations to subjects and examining their fall behaviors. Cable-driven robotic devices have been used for waist perturbation in balance [8], gait improvement [9], and rehabilitation studies [10], [11]. Compared to wearable robotic devices, they are versatile due to their ability to adapt to different human movements and add minimal weight to users. Even though cable-driven robotic devices for waist perturbation exhibit great benefits in studying balance recovery reaction [12], reducing human energetic consumption [13] or improving gait functions [14], the hardware design and control approach development would have higher requirements to achieve desired outcomes.

A major component of these devices' development is the control strategy, which enables the device to effectively track the force applied to the subject and ensure a controllable, safe, and permissible range of operation. From the state-of-the-art studies, most of these devices use proportional-integral-derivative (PID) controllers, as described in [15], which requires careful PID control gains tuning before achieving an acceptable force control performance. Another study employed a quadratic programming-based optimization scheme to determine the optimal cable tension, which serves as feedback for a PID controller [16]. Existing studies [15], [17], [18], typically focus on the constant horizontal force applied on the trunk and evaluate the effects on the user's gait, biomechanics, and energetics. Under this scenario, known as a regulation problem in the control field, a traditional PID-type control is usually applied without considering the system dynamics or time-varying characteristics of the horizontal cable force reference. Therefore, it cannot address challenges in real experimental scenarios, such as non-linearity, human-robot interaction, and so on.

In this study, we developed a modular cable-driven robotic platform suitable for studying human balance and gait characteristics. This device can administer various force profiles, a magnitude of up to 120 N, and a minimal rise time of 29

*This work was supported by the FOAP at the University of Alabama #13009-214271-200. Corresponding author: Qiang Zhang (qiang.zhang@ua.edu).

[1]O. Akinniyi and Q. Zhang are with the Department of Mechanical Engineering, the University of Alabama, Tuscaloosa, AL 35401, USA. Q. Zhang is also with the Department of Chemical and Biological Engineering, the University of Alabama, Tuscaloosa, AL 35401, USA.

[2]M. Sharifi is with the Department of Mechanical Engineering, San Jose State University, San Jose, CA 95192, USA.

[3]D. Martelli is with the Orthopedics/Sports Medicine Department, MedStar Health Research Institute, Baltimore, MD 21218, USA.

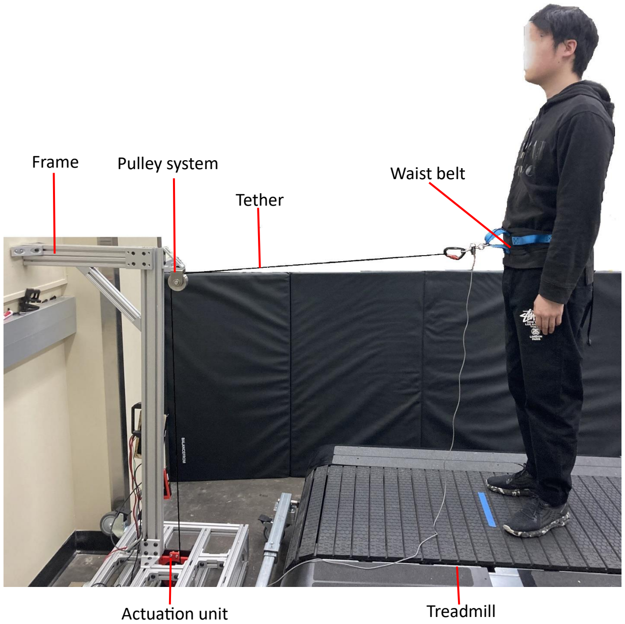

Fig. 1: The system setup. A subject standing on the treadmill with the cable connected from the actuation unit to the waistbelt. The device frame is attached to the wall.

ms for a unit step reference input. To improve end-effector force tracking performance, we developed a closed-loop adaptive Kalman filter-based full-state feedback controller with the reference input. The control gains were first carefully designed in a simulation study, where a linear dynamic model between the input voltage and output cable force was identified. Then, the same control gains were applied to the experimental studies, where we tested the performance of the controller with different force profiles using a fixed object, and human subjects in standing and walking conditions. This study is focused on the performance testing of the robotic platform and the developed controller.

II. Mechatronics Design of the Cable-Driven Robotic Platform

A. Structural design

We developed a cable-driven robotic platform shown in Fig. 1, capable of applying pulling force at the subject's COM (around the waist). The system setup, including the actuation unit, controller, and other hardware components, is illustrated in Fig. 2. The actuation unit is housed in a 3D-printed case and mounted on a rolling base attached to a T-slotted frame. The frame can be easily assembled and disassembled, with screws for wall attachment. A lightweight force sensor connects the waistbelt to a cable, which passes through a pulley to a direct-drive EC motor. A breakaway cable ensures subject safety by disconnecting in case of excessive force. An emergency button stops system operation in case of malfunction.

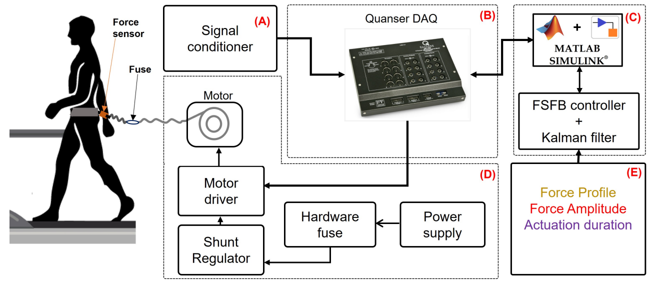

Fig. 2: The system overview. (A) The sensing unit amplifies, and conditions input voltage from the force sensor; (B) The input-output data acquisition unit integrates the sensing and actuation units to the controller on the computer system; (C) The full state feedback controller with reference input and the Kalman filter tracks the reference force; (D) The actuation unit transfers torque to the cable connected to the waist.

B. Actuation unit

A computer system with Matlab Simulink (MathWorks, Natick, MA, USA) software controlled actuation signals through a control unit (Quanser Q8-USB, ON, Canada) to drive an EC-motor (EC 90, Maxon Group, Switzerland) actuator. Forward force profiles were generated using an EC 90 motor (ESCON 70/10, Maxon Group, Switzerland) powered by a 48-volt DC power supply (RSP200048, Mean-well, Taiwan). A motor driver (ESCON 70/10, Maxon Group, Switzerland) with a series-connected shunt regulator (DRS 70/30, Maxon Group, Switzerland) manages motor control and current dissipation. The force from the actuator is transmitted via a 1.1 mm diameter cable with a breaking strength of 890 N. A 3D-printed flange shaft coupler and spool drum assembly prevent cable tangling during spooling. The EC motor is mounted on a 3D-printed frame bolted to a T-slotted (80/20, IN, USA) aluminum frame. An adjustable pulley (3211T32 Macmaster Carr, USA) attached to the T-slotted frame allows for angle adjustment of the applied force. Forces are applied to participants using a waist belt positioned to align with the subject's center of mass [18].

C. Sensing system

Applied forces to subjects were measured using a lightweight load cell (MLP-50, Transducer techniques, CA, USA). The load cell was mounted at the attachment point (waist belt) with the subject. This configuration eliminates oscillations or movements in the cable component during force measurement, ensuring that the measured force accurately represents the force applied at the waist belt without any additional influence from the cable's movement. Similar configurations were used in [15], [16], while others placed the load cells away from the attachment point [10], or determined the forces using a compression spring [9]. Analog voltages measured by the loadcell are filtered with a 2nd-order Butterworth filter at a cutoff frequency of 50 Hz using a signal conditioner (Flintec EA250 analog amplifier, MA, USA). The conditioned voltages are read by a computer system through the input port of a data acquisition system

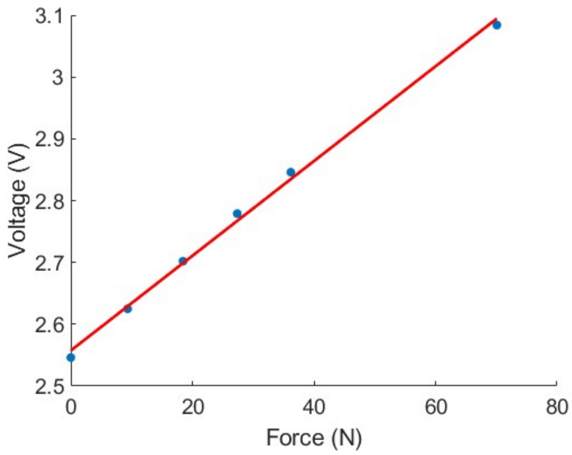

Fig. 3: The load cell calibration result plot.

(DAQ) (Quanser Q8-USB, ON, Canada). The load cell and signal conditioner were powered by a 24V DC workbench power supply.

III. System Identification of the Dynamic Model

We calibrated the load cell to ensure an accurate reading of the measured force during experiments. These measurements are essential for assessing the effectiveness of the perturbation applied to the subject's waist. Additionally, we developed an adaptive controller capable of dynamically adjusting to changes in the subject's movement patterns. The controller's output voltage to the motor is instrumental in controlling the perturbation intensity or timing, thereby ensuring optimal responsiveness. To ensure safety during experiments, we included additional safety bounds in the controller design.

A. Load cell calibration

An experimental test was done to calibrate the load cell, with the aim of ensuring precise and reliable measurements of the forces exerted on subjects' waist during perturbation, and to maintain these forces within safe limits. The load cell was fixed to a vertical beam at the top and a screw eye to the opposite end of the load cell. To apply the load, eight steel blocks were used, and the mass of the blocks including the screw eye was measured with a force plate (AMTI, MA, USA), all have a mass of 17.2 kg.

First, the initial reading was taken from the load cell without adding any loading as a baseline measurement. Then, the steel blocks were added progressively, while the load cell reading was recorded. The recorded load cell readings and the added reference loading weights represent the load cell's response to varying loads, which is demonstrated in Fig. 3. Considering the maximum applied horizontal force on the waist reported in the literature, we selected the first 12 points and calculated the linear relationship between the load cell output voltage and applied reference force. The linear equation was further used in force tracking control design and results analysis in subsequent sections.

TABLE I: Pseudo-code algorithm used for SI

Input:	Input SISO data into Matlab SI toolbox
Step 1:	Plot and process data
Step 2:	Estimate linear models using quick start tool
Step 3:	Select model with the best fit
Step 4:	Estimate transfer function models
Step 5:	Determine nominal transfer function model

B. Voltage input vs. load cell measurement identification

To determine the system step response, a set of customized codes was written in Matlab-Simulink which sends step input signals through the DAQ to the actuator of the cable-driven robotic system and applies a force through the cable on a hard-fixed object. The DAQ simultaneously reads the equivalent force measured by the load cell at the end-effector at a sampling frequency of 500 Hz. Step inputs of magnitudes ranging from 0.5 V to 13 V, increasing by 0.5 V increments were applied to the system to examine its step response. For each step input applied to the system, the resulting load cell measured force was saved on a spreadsheet. We used the system identification (SI) toolbox in Matlab to estimate and validate linear models from the single-input/single-output (SISO) system acquired from the step response test. The goal is to find a model that best describes the system's dynamics. The collected data samples were imported into the Matlab workspace using the SI toolbox. Each signal channel of the SISO system was plotted and processed, removing offsets from the data. After processing, the data was used for quick model estimation and validation using the SI quick start tool. The model-based output signal and the measured force signal were plotted and compared to determine the best-fit model under each step input condition. After adjusting the numbers of zeros and poles of the transfer function in the SI toolbox, we found the best-fit transfer function model contained 3 poles and no zeros. Therefore, we selected the same format for all transfer functions under different step input conditions. The algorithm used for the system identification is presented in Table I.

We calculated the average value of the corresponding coefficients of each term across a group of transfer functions obtained from the step response of the system and determined the nominal transfer function model as

$$T(s) = \frac{1480000}{s^3 + 75.472s^2 + 4212s + 127000}. \tag{1}$$

IV. Kalman Filter-based Full-State Feedback Control with Reference Input

The identified third-order nominal dynamic model in (1) can be represented as the state space equation form as

$$\begin{aligned} \dot{x} &= \begin{bmatrix} 0 & 1 & 0 \\ 0 & 0 & 1 \\ -127000 & -4212 & -75.472 \end{bmatrix} x + \begin{bmatrix} 0 \\ 0 \\ 1480000 \end{bmatrix} u \\ y &= \begin{bmatrix} 1 & 0 & 0 \end{bmatrix} x, \end{aligned} \tag{2}$$

where state variables are defined as $x = [f, \dot{f}, \ddot{f}]^T$ and f is the force measurement from the load cell.

If all state variables are available and reliable from some kinds of sensors, we can define the full state feedback control law of a linear combination of the state variables, that is

$$u(t) = -Kx(t) = -[k_1, k_2, k_3][x_1, x_2, x_3]^T, \tag{3}$$

where k_1, k_2, and k_3 are the control gains. However, for the real dynamic system in (1), the available reliable measurement is the force signal from the load cell, while the first-order and second-order time derivatives of the force signal are relatively noisy and can easily deteriorate the controller performance. To address the unmeasurable state variables issue, a Kalman filter with the nominal third-order linear model was used to get the estimates of state variables, x_1, x_2, and x_3, to be used for the full-state feedback control design. Then the new full state feedback control law is given as $u(t) = -[k_1, k_2, k_3][\hat{x}_1, \hat{x}_2, \hat{x}_3]^T$. The proposed control diagram is demonstrated in Fig. 4. Typically, the general control law in (3) does not consider a reference input, and it could lead to steady-state error easily. Therefore, it is required to compute the steady-state values of the state and control input that will result in zero output error and then force them to take these values.

In the current control development, assume the desired final (steady-state) values of the state and the control input are $\hat{x}_{ss}$ and u_{ss}, then the new control law should be given as

$$u_{new}(t) = u_{ss} - K(\hat{x} - \hat{x}_{ss}), \tag{4}$$

where $u = u_{ss}$ as long as $\hat{x} = \hat{x}_{ss}$ (no state variable error). To select the correct final values, those equations must be solved so that the system will have zero steady-state error to any constant input. Recall the state space equation in (2), the steady-state condition can be written as

$$0 = A\hat{x}_{ss} + Bu_{ss}, y_{ss} = C\hat{x}_{ss}. \tag{5}$$

To solve for the values for which $y_{ss} = r_{ss}$ for any value of r_{ss}, some substitutions are given as $\hat{x}_{ss} = N_x r_{ss}$ and $u_{ss} = N_u r_{ss}$. Then the form in (5) can be written in a matrix format

$$\begin{bmatrix} A & B \\ C & 0 \end{bmatrix} \begin{bmatrix} N_x \\ N_u \end{bmatrix} = \begin{bmatrix} 0 \\ 1 \end{bmatrix}. \tag{6}$$

where the variables N_x and N_u in the equation above can be calculated below

$$\begin{bmatrix} N_x \\ N_u \end{bmatrix} = \begin{bmatrix} A & B \\ C & 0 \end{bmatrix}^{-1} \begin{bmatrix} 0 \\ 1 \end{bmatrix}. \tag{7}$$

With these values, the complete control law for introducing the reference input to get zero steady-state error is given as

$$u_{new} = N_u r_{ss} - K(\hat{x} - N_x r_{ss}) = -K\hat{x} + (N_u + KN_x) r_{ss}. \tag{8}$$

V. Experimental Results and Discussions

A. Experimental protocol

Three able-bodied participants (all male; mean age: 29.3 yrs) were recruited in the preliminary study. All participants are healthy with no musculoskeletal, neuromuscular, or major medical problems. All participants signed an informed consent form approved by the Medical Institutional Review Board of the University of Alabama (#21-06-4695-R2).

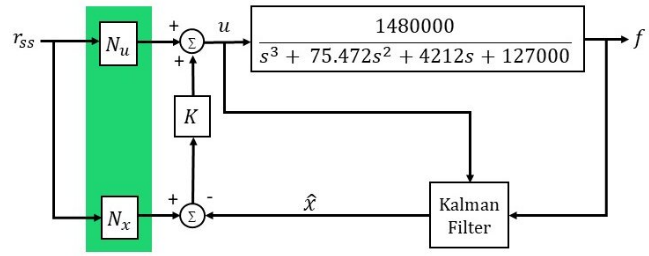

Fig. 4: The Control block diagram for introducing the reference input with full-state feedback.

We tested the proposed controller and a PID controller under three conditions: (C1) end-effector fixed-object conditions, (C2) human subject static standing conditions, and (C3) human subject treadmill walking conditions. The PID controller gains were manually tuned based on the experimenter's observation. For C1, the end-effector of the system was attached to a fixed-object structure placed 1.52 m away from the motor installation frame, and the cable was preloaded with a force of 2 N. Reference step and half-sinusoidal (only non-negative values included) forward pull force profiles (magnitude: 5 N to 80 N, sinusoidal signal frequency: 1 Hz) were programmed in Simulink, to generate the control command to the motor for the force tracking at the end-effector through the cable. For C2, the end-effector was attached to the waistbelt worn by human subjects. The same forward pull force profiles were applied to the subjects in the anterior position while standing approximately 1.52 m from the motor installation frame. For C3, a sinusoidal force profile (magnitude: 10 N, 20 N, and 30 N; frequency: 1 Hz) corresponding to the approximate walking step frequency of the subjects was applied to the waist while walking on the treadmill (Horizon Fitness, WI, USA) [9] at a fixed speed of 0.8 $miles/hour$. The subjects were asked to relax and not oppose the waist pull during the experiment. The following control parameters were used in the experimental study

$$K = \begin{bmatrix} 12.8924 & 0.1539 & 0.0005 \end{bmatrix},$$
$$N_u = 0.0858,$$
$$N_x = \begin{bmatrix} 1 \\ 0 \\ 0 \end{bmatrix}.$$

B. Results under multiple conditions

For each experimental condition, we recorded the reference force, measured force, and the controller output voltage to the motor. Given that we conducted many testing trials under the three conditions in the current study, we only provide some exampled end-effector force closed-loop performance here. As shown in Fig. 5, the step response to a 20 N reference signal was used to evaluate percentage overshoot, rise time, and steady-state errors across the three conditions, considering one subject in C2

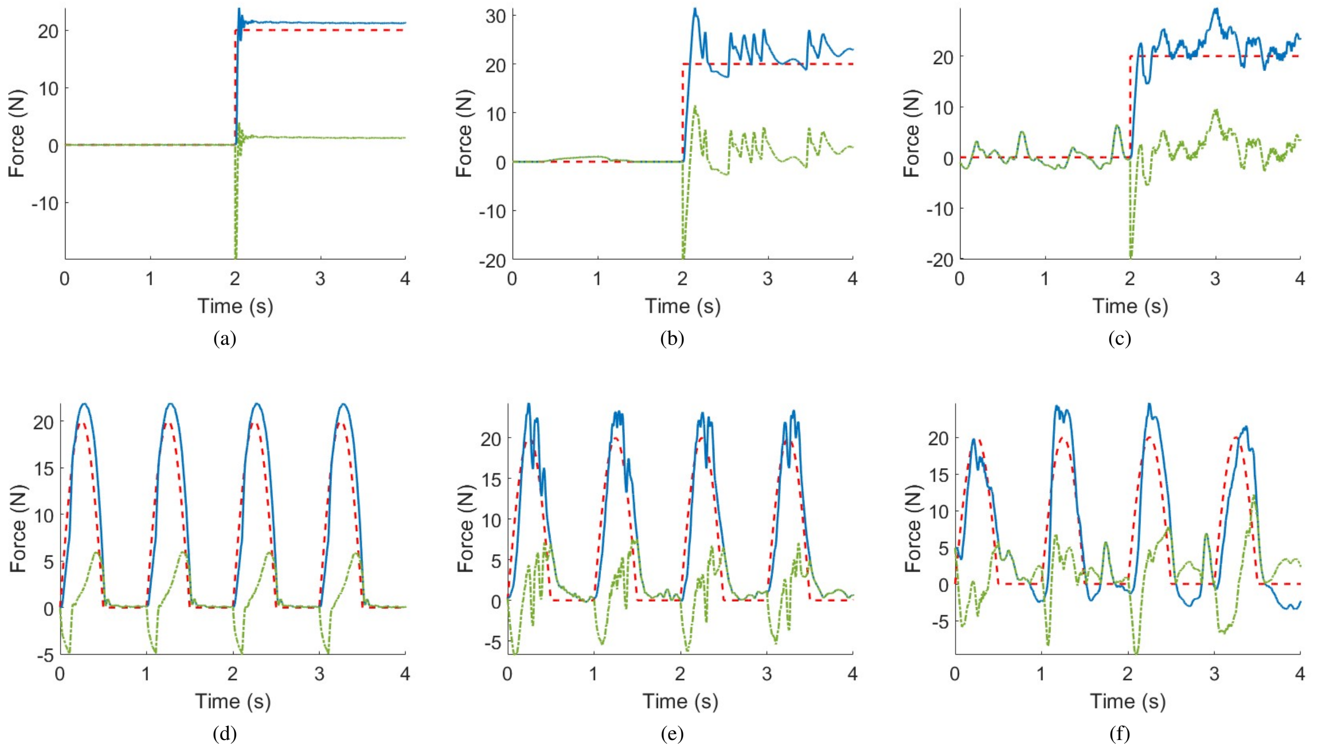

Fig. 5: Closed-loop force trajectory tracking under fixed-object, standing, and walking conditions. **(a)** Step response with end-effector fixed-object condition; **(b)** Step response with a subject standing; **(c)** Step response with a subject walking on a treadmill; **(d)** Sinusoidal response with an end-effector fixed-object condition; **(e)** Sinusoidal response with a subject standing; **(f)** Sinusoidal response with a subject walking on a treadmill. Red dashed lines (ref) represent desired force signals. Blue solid lines represent measured load cell force signals. Green dashed dot lines represent the errors between the desired and measured force data.

TABLE II: Force regulation performance with step reference input signals.

Step response with the three conditions with step input; C1 = fixed-object condition, C2 = standing condition, and C3 = walking condition. sse = steady-state error.

	magnitude	overshoot (%)	rise time (ms)	sse (%)
C1	20 N	19.4	32	5.9
	50 N	32.9	30	19.4
	80 N	34.1	29	4.8
C2	20 N	51.3 ± 8.8	80.0 ± 2.8	11.0 ± 4.2
	50 N	53.1 ± 4.7	73.0 ± 2.1	8.4 ± 2.3
	80 N	48.5 ± 1.5	66.0 ± 0.7	13.1 ± 8.1
C3	10 N	85.9 ± 12.4	98.0 ± 13.4	9.8 ± 10.6
	20 N	55.9 ± 7.2	74.7 ± 6.6	24.8 ± 13.3
	30 N	53.8 ± 8.8	84.0 ± 2.83	18.9 ± 24.0

TABLE III: Force tracking performance with sinusoidal reference input signals.

Results of the three conditions with sinusoidal reference signals; C1 = fixed-object condition, C2 = standing condition, C3 = walking condition. RMSE = Root Mean Square Error, RRMSE = RMSE/magnitude.

	magnitude	RMSE (N)	RRMSE (%)
C1	20 N	2.6	13.2
	50 N	6.9	13.8
	80 N	10.6	13.3
C2	20 N	3.4 ± 0.2	17.0 ± 1.0
	50 N	8.3 ± 0.2	16.6 ± 0.4
	80 N	12.7 ± 1.0	15.9 ± 1.3
C3	10 N	3.9 ± 2.2	39.0 ± 22.0
	20 N	5.1 ± 1.0	25.5 ± 5.0
	30 N	5.8 ± 0.7	19.3 ± 2.3

and C3. The percentage overshoots for conditions 1, 2, and 3 are 19.4%, 57.5%, and 47.7% respectively. Rise time in C1 for a magnitude of 20 N, was observed to be 32 ms. Under C2, the same magnitude profile exhibited a rise time of 80 ms. C3 resulted in a rise time of 81 ms, for the same magnitude. Regarding steady-state errors, in C1, a magnitude of 20 N yielded a value of 5.9%. For C2, the corresponding steady-state error is 8.0% with a magnitude of 20 N. C3 resulted in a steady-state error of 19.5% for a magnitude of 20 N. To assess the system's ability to track time-varying reference forces, we applied a sinusoidal signal of magnitude 20 N to the system under the three conditions, considering a subject in C2 and C3. In Conditions 1, 2, and 3, the system tracked the sinusoidal reference input with relative errors ($\frac{RMSE}{magnitude}*100$) of 13.2%, 17.6%, and 20.5%, respectively. Statistical results across all subjects and trials are presented in Tables II and III.

C. Discussions

A critical aspect of a human perturbation system is its ability to rapidly apply perturbation in less time than it takes for subjects to respond to a stimulus. Human response times are typically between 45 ms to 60 ms, with a stretch-reflex delay model suggesting approximately 90 ms [19]. Our system demonstrated high responsiveness, with a minimum rise time of 29 ms, making it suitable for perturbation in human balance and gait experiments. A Similar study attained a rise time of 44 ms [18]. Compared to conventional PID controllers, our controller showed higher responsiveness, achieving a rise time range of 29 ms to 32 ms for input magnitudes from 20 N to 80 N. The proposed controller demonstrates significant potential in terms of accuracy by efficiently regulating its behavior in response to disturbances. This capability is crucial for achieving reliable and safe results across different trials and experiments. This is evident in the reduction of the RMSE in both C1 and C2. Specifically, when tracking sinusoidal reference inputs ranging from 20 N to 80 N, the proposed controller achieved relative RMSE values between 13.2% and 13.8% in C1. In contrast, a PID controller yielded relative RMSE values between 25.8% and 26.8% under identical input magnitudes. Similarly, in C2, the proposed controller attained relative RMSE values ranging from 15.9% $\pm$ 1.3% to 17.0% $\pm$ 1.0% for the same range of input magnitudes. Conversely, the PID controller yielded considerably higher relative RMSE values, ranging from 35.6% $\pm$ 2.6% to 42.1% $\pm$ 3.6% under identical experimental conditions.

VI. Conclusion

In this work, we developed a cable-driven robotic platform for waist perturbation, designed an adaptive full-state-feedback control approach for cable force trajectory tracking, and evaluated the force control performance through benchtop testing and preliminary human subjects testing. The experimental results demonstrated reliable sinusoidal input force tracking outcomes across a range of magnitudes: 20 N, 50 N, and 80 N. In the end-effector fixed-object condition, the system showed consistent force-tracking outcomes with RMSE values of 2.6 N, 6.9 N, and 10.6 N respectively. In the human standing condition, RMSE values of 3.4 N $\pm$ 0.2 N, 8.3 N $\pm$ 0.2 N, and 12.7 N $\pm$ 1.0 N respectively were recorded. Moreover, during the human treadmill walking, RMSE values of 3.9 N $\pm$ 2.2 N, 5.1 N $\pm$ 1.0 N, and 5.8 N $\pm$ 0.7 N were recorded for force magnitudes of 10 N, 20 N, and 30 N respectively. These results show the system's adaptability and reliability across diverse experimental conditions, highlighting its potential for use in balance and gait experiments. Our next step will focus on the design of a hierarchical control framework to personalize the waist assistance level for 1) older adults with a control objective of maximizing gait balance or 2) healthy human users with a control objective of minimizing lower-limb muscle contraction activities while walking on the treadmill.

Aknowledgement

The authors extend their gratitude to Matthew Grosman for his assistance with all the 3D design and printing used in this work.

References

[1] T. Masud and R. O. Morris, "Epidemiology of falls," *Age and ageing*, vol. 30, no. suppl_4, pp. 3–7, 2001.
[2] W. P. Berg, H. M. Alessio, E. M. Mills, and C. Tong, "Circumstances and consequences of falls in independent community-dwelling older adults," *Age and ageing*, vol. 26, no. 4, pp. 261–268, 1997.
[3] C. S. Florence, G. Bergen, A. Atherly, E. Burns, J. Stevens, and C. Drake, "Medical costs of fatal and nonfatal falls in older adults," *JAGS*, vol. 66, no. 4, pp. 693–698, 2018.
[4] J. L. Kelsey, E. Procter-Gray, M. T. Hannan, and W. Li, "Heterogeneity of falls among older adults: implications for public health prevention," *Am. J. Public Health*, vol. 102, no. 11, pp. 2149–2156, 2012.
[5] S. N. Robinovitch, F. Feldman, Y. Yang, R. Schonnop, P. M. Leung, T. Sarraf, J. Sims-Gould, and M. Loughin, "Video capture of the circumstances of falls in elderly people residing in long-term care: an observational study," *The lancet*, vol. 381, no. 9860, pp. 47–54, 2013.
[6] E. Aartolahti, E. Lönnroos, S. Hartikainen, and A. Häkkinen, "Long-term strength and balance training in prevention of decline in muscle strength and mobility in older adults," *Aging Clin. Exp. Res.*, vol. 32, pp. 59–66, 2020.
[7] J. Hamm, A. G. Money, A. Atwal, and I. Paraskevopoulos, "Fall prevention intervention technologies: A conceptual framework and survey of the state of the art," *J. Biomed. Inform*, vol. 59, pp. 319–345, 2016.
[8] Y.-C. Pai, M. W. Rogers, J. Patton, T. D. Cain, and T. A. Hanke, "Static versus dynamic predictions of protective stepping following waist–pull perturbations in young and older adults," *J. Biomech.*, vol. 31, no. 12, pp. 1111–1118, 1998.
[9] S. N. Simha, J. D. Wong, J. C. Selinger, and J. M. Donelan, "A mechatronic system for studying energy optimization during walking," *IEEE Trans. Neural Syst. Rehabil. Eng.*, vol. 27, no. 7, pp. 1416–1425, 2019.
[10] V. Vashista, D. Martelli, and S. K. Agrawal, "Locomotor adaptation to an asymmetric force on the human pelvis directed along the right leg." *IEEE Trans. Neural Syst. Rehabil. Eng.*, 2015.
[11] B. Zi, G. Yin, and D. Zhang, "Design and optimization of a hybrid-driven waist rehabilitation robot," *Sensors*, vol. 16, no. 12, p. 2121, 2016.
[12] D. Martelli, J. Kang, F. Aprigliano, U. M. Staudinger, and S. K. Agrawal, "Acute effects of a perturbation-based balance training on cognitive performance in healthy older adults: A pilot study," *Front. Sports Act. Living.*, vol. 3, p. 688519, 2021.
[13] X. Tang, X. Wang, X. Ji, Y. Zhou, J. Yang, Y. Wei, and W. Zhang, "A wearable lower limb exoskeleton: Reducing the energy cost of human movement," *Micromachines*, vol. 13, no. 6, p. 900, 2022.
[14] P. K. Jamwal, S. Hussain, and M. H. Ghayesh, "Robotic orthoses for gait rehabilitation: An overview of mechanical design and control strategies," *Proceedings of the Institution of Mechanical Engineers, Part H: J. Med. Eng*, vol. 234, no. 5, pp. 444–457, 2020.
[15] A. M. Gonabadi, P. Antonellis, and P. Malcolm, "A system for simple robotic walking assistance with linear impulses at the center of mass," *IEEE Trans. Neural Syst. Rehabil. Eng.*, vol. 28, no. 6, pp. 1353–1362, 2020.
[16] V. Vashista, X. Jin, and S. K. Agrawal, "Active tethered pelvic assist device (a-tpad) to study force adaptation in human walking," in *2014 IEEE international conference on robotics and automation (ICRA)*. IEEE, 2014, pp. 718–723.
[17] C. A. Zirker, B. C. Bennett, and M. F. Abel, "Changes in kinematics, metabolic cost, and external work during walking with a forward assistive force," *J. Appl. Biomech*, vol. 29, no. 4, pp. 481–489, 2013.
[18] G. R. Tan, M. Raitor, and S. H. Collins, "Bump'em: an open-source, bump-emulation system for studying human balance and gait," in *2020 IEEE International Conference on Robotics and Automation (ICRA)*. IEEE, 2020, pp. 9093–9099.
[19] H. L. More and J. M. Donelan, "Scaling of sensorimotor delays in terrestrial mammals," *Proceedings of the Royal Society B*, vol. 285, no. 1885, p. 20180613, 2018.